Synthesis, characterization, and *in vivo* evaluation of the anticancer activity of a series of 5- and 6-(halomethyl)-2,2'-bipyridine rhenium tricarbonyl complexes.

Sara Nasiri Sovari[a], Isabelle Kolly[a], Kevin Schindler[a], Ana Djuric[b], Tatjana Srdic-Rajic[b], Aurelien Crochet[a], Aleksandar Pavic[c*], Fabio Zobi[a*]

[a]Department of Chemistry, University of Fribourg, Chemin du Musée 10, 1700 Fribourg, Switzerland.

[b]Department of experimental oncology, Institute for Oncology and Radiology of Serbia, Pasterova 14, Beograd, Republic of Serbia

[c]Institute of Molecular Genetics and Genetic Engineering, University of Belgrade, Vojvode Stepe 444a, 11000 Belgrade, Republic of Serbia.

*To whom all the correspondence should be addressed.

Phone (+381) 11 397 60 34, Fax (+381) 11 397 58 08, E-mail: sasapavic@imgge.bg.ac.rs

Phone (+41) 26 300 87 85, Fax (+41) 26 300 97 37, E-mail: fabio.zobi@unifr.ch

Abstract

We report the synthesis, characterization, and *in vivo* evaluation of the anticancer activity of a series of 5- and 6-(halomethyl)-2,2'-bipyridine rhenium tricarbonyl complexes. The study was promoted in order to understand if the presence and position of a reactive halomethyl substituent on the diimine ligand system of *fac*-$[Re(CO)_3]^+$ species may be a key molecular feature for the design of active and non-toxic anticancer agents. Only compounds potentially able of ligand-based alkylating reactions show significant antiproliferative activity against colorectal and pancreatic cell lines. The anticancer potency of the species, does not correlate with the hydrolysis rate or rate of reaction of the coordinated 5- and 6-(halomethyl)-2,2'-bipyridine with the amino acid lysine. Of the new species presented in this study, one compound (5-(chloromethyl)-2,2'-bipyridine derivative) shows significant inhibition of pancreatic tumour growth *in vivo* in zebrafish-Panc-1 xenografts. The complex is noticeably effective at 8 μM concentration, lower than its *in vitro* IC_{50} values, being also capable of inhibiting *in vivo* cancer cells dissemination.

Keywords:
rhenium, anticancer, pancreatic tumour, colorectal carcinoma, zebrafish, xenograft.

1. Introduction

Cisplatin is well known for being the first metallodrug for treatment of neoplastic diseases [1], but after gaining clinical success, its use was limited due to the emergence of side effects (e.g., inherent nephrotoxicity and ototoxicity). The discovery of cisplatin, however, has ignited a thriving field of research, with several medicinal inorganic chemists now exploring the potential anticancer efficacy of other transition metal species. Classic platinum(II) and new platinum(IV) complexes still dominate the literature [2] with ruthenium, copper and gold being other prominent examples [3-5]. Rhenium(I) tricarbonyl complexes are amongst the least explored in the field, but in the last decade have gained significant attention due to their unique and promising properties, which include high stability, low toxicity and rich spectroscopic and luminescent features. The surprising number of recent reviews [6-15] on the anticancer potential of Re species corroborates the interest around such complexes.

Apart from the constant *fac*-$[Re(CO)_3]^+$ core, little is known about what molecular features may be commonly required for an active compound. An examination of the published contributions in the field, generally indicates that the cytotoxicity of Re(I) tricarbonyl complexes positively correlates with lipophilic properties of the species [16-20], which is associated with an improved passive cellular uptake. Different Re(I) tricarbonyl molecules possessing neoplastic activities (often with *in vitro* anti-proliferative potency higher than cisplatin [14]) act by different mechanisms of action, including mitochondrial [21-25] or enzymatic inhibition [26], DNA interaction [27-30] or endoplasmic reticulum (ER) stress [31]. Of the different complexes published to date, a few molecules are, in our view, of particular interest, because they have been studied in more details *in vivo*. These are the tricarbonyl rhenium isonitrile polypyridyl (TRIP) complex of Wilson *et al.*, the diseleno-ether compound of Collery *et al.* (diSe-Re in Chart 1) and the the *N*-heterocylic carbene complex (NHC-Re, Chart 1) of Falasca *et al.*

TRIP exhibits potent *in vitro* anticancer activity in a variety of cell lines (IC_{50} value 1.4–1.9 μM) and acts by triggering the accumulation of misfolded proteins, which causes endoplasmic reticulum (ER) stress, unfolded protein response, and apoptotic cell death in addition to mitochondrial fission [31]. The compound remains intact *in vitro* as demonstrated by x-ray fluorescence microscopy (XFM) [32], and when administered in NSG mice bearing A2780 ovarian cancer xenografts (20 mg/kg twice weekly), it is able to inhibit tumor growth and prolong mouse survival by 150% compared to control [33]. DiSe-Re exhibits activities against several solid tumor cell lines [34] and a potent inhibitory effect on breast cancer MDA-MB231 cell division [35]. Moreover, diSe-Re promotes *in vivo* (10 mg/kg/d) a remarkable

reduction of tumors volume in mice-bearing a MDA-MB231 Luc+ xenografts and pulmonary metastases without signs of clinical toxicity [35]. The compound acts as an anti-oxidant agent (decreasing ROS production) and significantly decreases the levels of the transforming growth factor beta 1 (TGF- β1), vascular endothelial growth factor A (VEGF-A) and insulin-like growth factor 1 (IGF-1) [36, 37]. NHC-Re shows low μM activity against pancreatic cancer cell lines where it induces cell cycle arrest at the G2/M phase by inhibiting the phosphorylation of Aurora-A kinase [38], and blocks growth of aggressive cancers *in vivo* (mice bearing HPAF-II human pancreatic cancer xenografts) by inhibiting FGFR- and SRC-mediated signaling [39].

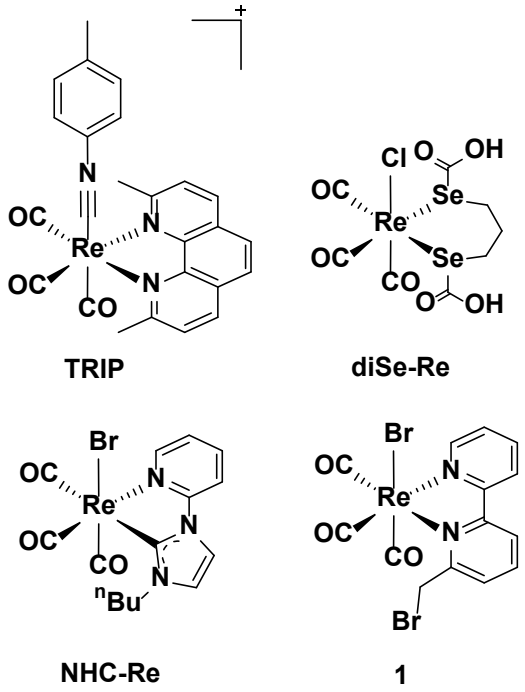

Chart 1. Selected structures of anticancer Re complexes evaluated *in vivo*.

We have also been interested in the development of antibiotic [40] and anticancer rhenium species [41]. In a recent study, we have reported the anti-proliferative efficacy of a series of *fac*-$[Re(I)(CO)_3]^+$ N-derivatized N-([2,2'-bipyridin]-6-ylmethyl)-species against colorectal carcinoma (CRC) and identified complex **1** (Chart 1) as a potent *in vivo* (zebrafish xenograft model of human CRC) anticancer, anti-angiogenic and antimetastatic compound [42]. *In vivo*, compound **1** (1-3 μM concentration) is more potent than clinical drugs, such as cisplatin and sunitinib malate, and shows no signs of clinical toxicity (cardio-, hepato- , and myelotoxicity) at high concentrations (i.e., 250 μM).

The identification of **1** amongst a series of related species, made us wonder if the presence and position of a reactive halomethyl substituent on the diimine ligand system of *fac*-

$[Re(CO)_3]^+$ core may be a/the key molecular feature for the activity of **1** and for design of similar active and non-toxic anticancer agents. After all, **1** is of a relatively simple design, not dissimilar from other diimine rhenium compounds that, however, do not appear to be as promising as **1**, and the presence of the reactive halomethyl substituent is the unique feature of **1** in the series of compounds investigated. To this end, we have prepared a small library of 5- and 6-(halomethyl)-2,2'-bipyridine rhenium tricarbonyl complexes, and evaluated *in vivo* their anticancer activity against pancreatic and CRC tumors. Of the new species presented in this study, only one compound (5-(chloromethyl)-2,2'-bipyridine derivative) shows significant inhibition of pancreatic tumour growth in zebrafish-Panc-1 xenografts. The complex is also capable of inhibiting *in vivo* cancer cells dissemination, but it does not surpass the genuine potential of **1**. We describe our findings in the following sections.

2. Results and discussion

2.1. Chemistry

Ligands and rhenium complexes **1-10** were prepared according to the synthetic protocols illustrated in Scheme 1. The 2,2'-bipyridine derivatives were obtained *via* the well-established Pd-catalyzed Stille's C-C coupling reaction [43], starting from commercially available reagents. The 5- and 6-(difluoromethyl)-2,2'-bipyridines (**L_5** and **L_{10}** in Scheme 1) were obtained in a single step in moderate yields of 17 % and 38 % respectively. Similarly [2,2'-bipyridin]-5- and 6-ylmethanol (**L_3** and **L_8**) were obtained in good yield from the corresponding methyl [2,2'-bipyridine]-#-carboxylate following its reduction with $NaBH_4$. Ligands **L_3** and **L_8** were then converted to the 5- and 6-(halomethyl)-2,2'-bipyridines (**L_1**, **L_2**, **L_6** and **L_7**) either by treatment with PBr_3 (**L_1** and **L_6**) or thionyl chloride (**L_2** and **L_7**). Finally, the rhenium complexes were obtained in high yield by treatment of *fac*-$[Re(CO)_5Br]$ with the corresponding 2,2'-bipyridine ligand in hot toluene [42] (Scheme 1).

^1H NMR spectra of complexes (ESI, Figure S1-S9) showed pure diamagnetic compounds, according to the symmetry given by the facial-arranged CO's and low-spin d^6 nature of the metal ion. IR spectroscopy analysis was in accordance with the typical tricarbonyl vibration pattern. Crystals suitable for X-ray diffraction analysis were obtained for seven of nine new species. Crystallographic details are given in ESI, whereas Figures 1 and 2 depict respectively the ORTEPs of the *meta*- and *ortho*- substituted derivative. Complexes **2**, **6**, **7**, **9** and **10** all crystallized in a monoclinic lattice and space groups C2/c (**2**), P21/c (**6**, **7** and **10**), Pc (**9**) respectively, whereas **3** and **5** were obtained in the triclinic space group P-1 and in the orthorhombic space group Pca21. All seven crystal structures of the complexes (Figures 1 and

2) present a slightly distorted octahedral geometry around the central metal ion, but structural parameters are not significantly different from similar *fac*-$[Re(CO)_3]^+$ species (CCDC search). Spectroscopically, **2-10** show the characteristic stretching bands expected for tricarbonyl complexes in the water-free region of their IR spectra. For all complexes, as predicted [44], the pattern is very similar both in terms of frequency and in intensity of the stretching vibration. The UV-Vis spectra of the compounds display two main absorptions. All complexes show similar $\pi \rightarrow \pi^*$ intra-ligand transitions (LLCT) as sharp bands in at 300 nm attributed to the diimine-ligand system. In addition, the spectra show a metal-to-ligand charge transfer transition (MLCT, responsible for the luminescent properties of the species) cantered at 370 nm [45].

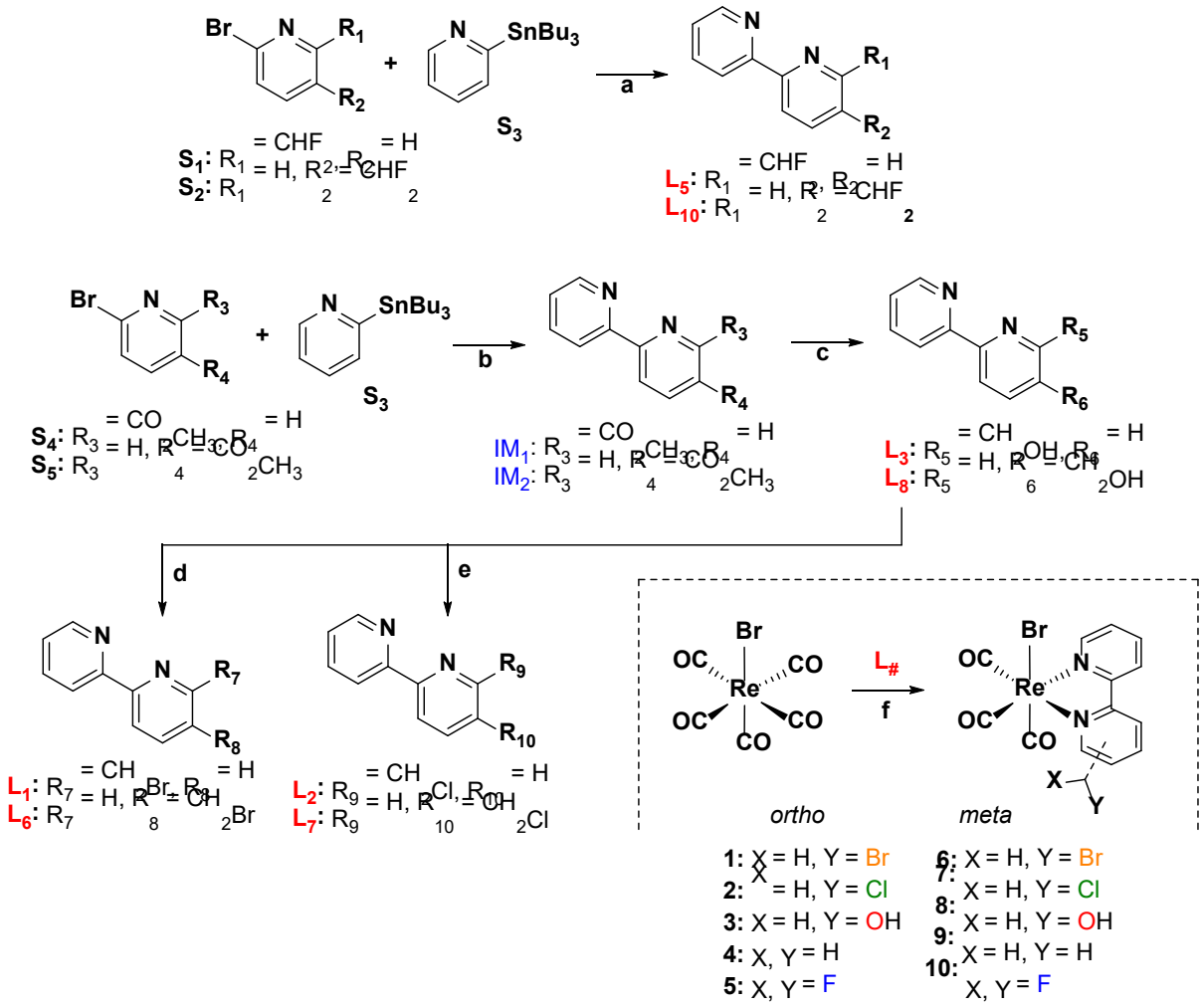

Scheme 1. Synthesis and chemical structures of bipyridine ligands ($L_{\#}$) and of Re complexes (bottom left). Conditions: (a) & (b) $Pd(PPh_3)_2(Cl)_2$, dry DMF, 130 °C, 10h, under argon, 17-41 %; (c) $NaBH_4$, Ethanol, H_2O, 85 °C, 3h, under argon, 76-79 %; (d) PBr_3, dry DCM, rt, 10h, under argon, 77-89 %; (e) $SOCl_2$, $NaHCO_3$, 80°C, 2h, 80-83 %, (f) a) Toluene, 85-100 ºC, 10-12h, 68-96 %.

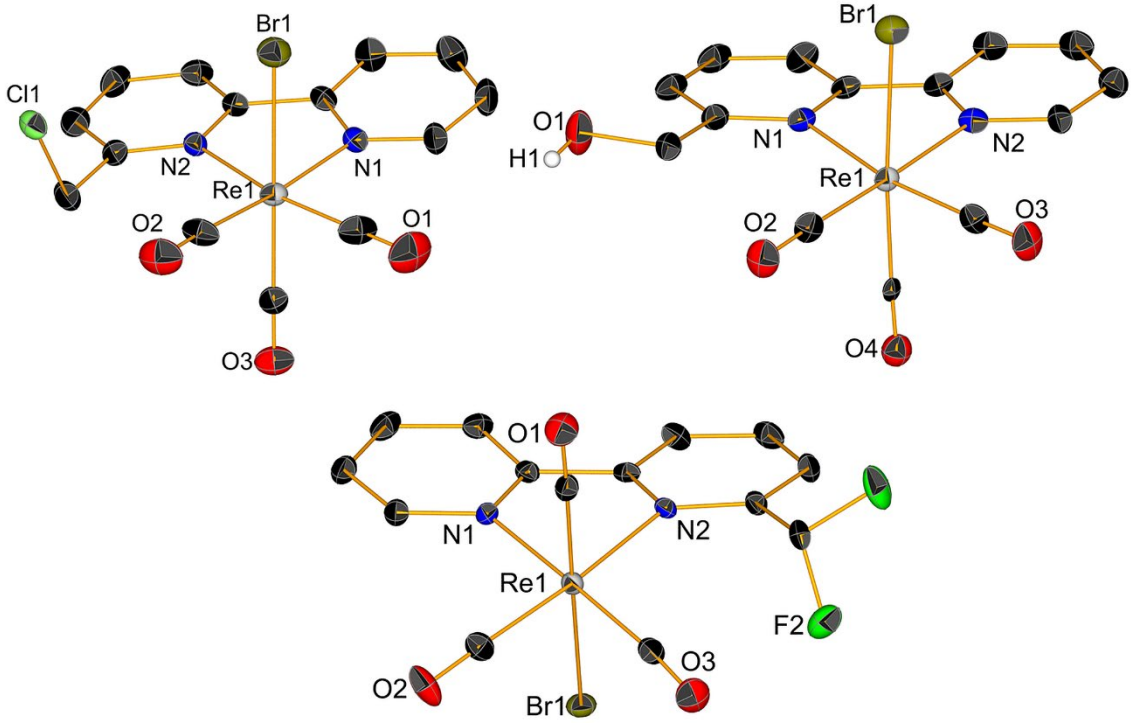

Figure 1. Crystal structures of compounds **2**, **3** and **5**. Thermal ellipsoids are at 30% probability. Hydrogen atoms are omitted for clarity.

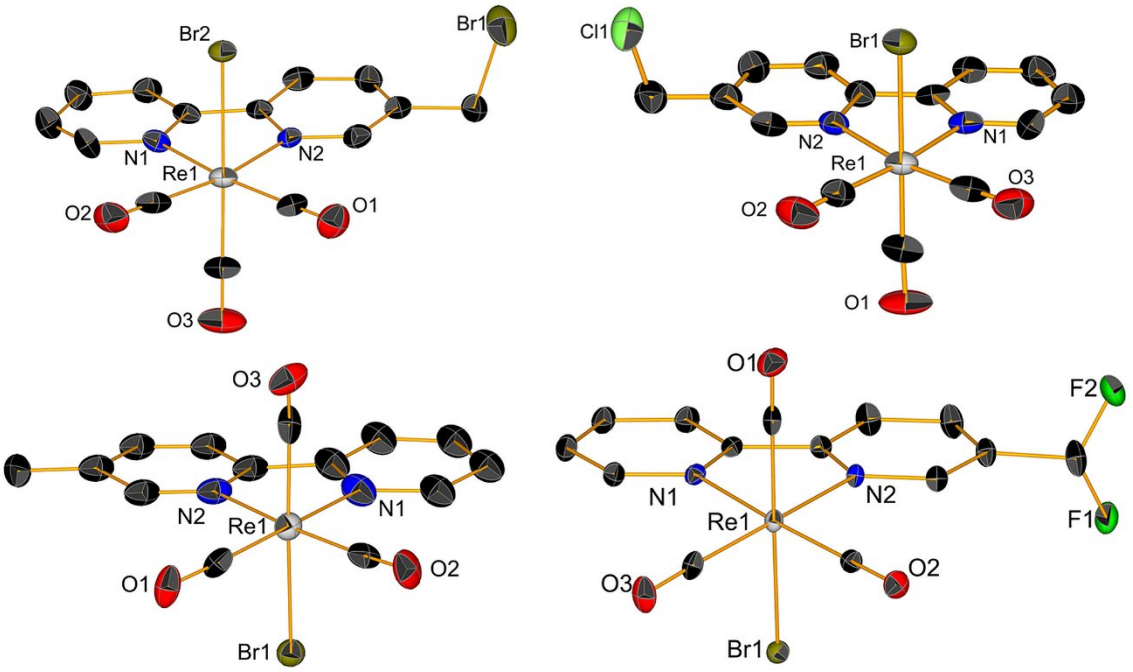

Figure 2. Crystal structures of compounds **6**, **7**, **9** and **10**. Thermal ellipsoids are at 30% probability. Hydrogen atoms are omitted for clarity.

2.2 Relative lipophilicity of complexes

The activity of rhenium tricarbonyl anticancer drugs is often correlated to their lipophilicity [10, 46-51]. The lipophilicity of the complexes is generally defined by octanol-water partition coefficient (logP, or K_{ow} value) referring to the ratio of the compound's concentration in the octanol phase to its concentration in the aqueous phase in the two-components system. Although previously we did not see a correlation between the lipophilicity and IC_{50} values of 6-(methyl-derivatized)-2,2'-bipyridine *fac*-$[Re(CO)_3]^+$ compounds, we decided to calculate and provide drug-likeness data of the complexes presented herein. We believe it is important to add such data in an era of computer-aided drug design of metal-based drug discovery. The drug-likeness properties of compounds **1-10** were calculated via the Molinspiration software. The results are given in Table 1. Complexes, overall, show very similar lipophilicity with the chloro and bromo derivatives (i.e. compounds **1**-**2** and **6**-**7**) being the most lipophilic species and the hydroxo derivatives (**3** and **8**) the most hydrophilic. With the exception of their molecular weight, molecules rate well in the drug-likeness assessment (Table 1).

Table 1. Calculated molecular properties of investigated compounds for the assessment of drug-likeness.

Complex	miLogP[a]	TPSA[b]	M_W[c]	N_{atoms}[d]	N_{ON}[e]	N_{OHNH}[f]	N_{viol}[g]	N_{rotb}[h]	Vol.[i]
1	3.78	61.08	602.28	22	5	0	1	4	297.04
2	3.65	61.08	557.83	22	5	0	1	4	292.69
3	2.41	81.31	539.38	22	6	1	1	4	287.17
4	3.06	61.08	523.38	21	5	0	1	3	278.91
5	3.61	61.08	559.36	23	5	0	1	4	289.04
6	3.88	61.08	602.28	22	5	0	1	4	297.04
7	3.75	61.08	557.83	22	5	0	1	4	292.69
8	2.51	81.31	539.38	22	6	1	1	4	287.17
9	3.62	61.08	523.38	21	5	0	1	3	278.91
10	3.71	61.08	559.36	23	5	0	1	4	289.04

[a] Octanolewater partition coefficient (logP value obtained using Molinspiration method). [b] Molecular polar surface area in $Å^2$. [c] Molecular weight. [d] Number of nonhydrogen atoms. [e] Number of hydrogen-bond acceptors (O and N atoms). [f] Number of hydrogen-bond donors (OH and NH groups). [g] Number of "Rule of five" violations. [h] Number of rotatable bonds. [i] Molecular volume in $Å^3$.

2.3 *In vitro* anticancer activity evaluation

The antiproliferative effect of compounds **2**-**10** was evaluated on a panel of four cancer cell lines (2 colorectal and 2 pancreatic) and compared to the previously reported activity of **1**. In addition, the toxicity of all new complexes was assessed on a normal cell line (MRC-5) in order to determine the selectivity index (Si) of the molecules. Table 2 presents the results of

our analysis. As evident from the data, the potentially alkylating (i.e. "*reactive*") chloro- and bromomethyl complexes **2**, **6** and **7** showed higher antiproliferative activity, as compared to the *unreactive* complexes. Of these latter species, only **4** (i.e. the 6-methyl-2,2'-bipyridine complex) revealed comparable activity to **2**, **6** and **7**. As it is the case for **1**, the compounds are particularly effective against the colorectal HCT-116 cell line, with IC_{50} values ranging from ca. 5 to 10 μM. We consider this result of particular relevance since HCT-116 is a CRC cell line that rapidly acquires resistance to clinical anticancer drugs, including cisplatin, oxaliplatin, docetaxel, 5-FU, and others [52-55]. As we have previously pointed out [42], it is possible that unique characteristics of HCT-116 cells, including mutation in the KRAS proto-oncogene, exhibitions of wild-type p53 expression, stem cell-like properties, low differentiation level, fast division as well as epithelial morphology [55-57], could all be factors contributing to their higher sensitivity of tumor line this class of rhenium tricarbonyl complexes. Unlike **1**, however, the new compounds show in general a lower Si (Table 2) towards cancer cells, being only ca. twice as active when compared to the IC_{50} value against healthy MRC-5 cells. Only complex **7** showed moderately good selectivity towards HCT-116 with an Si of 3.1. Nevertheless, we decided to further investigate *in vivo* selected compounds with acceptable Si (here defined as Si > 1).

Table 2. *In vitro* cytotoxicity (IC_{50}, μM) and *in vivo* toxicity (LC_{50}, μM) of complexes **1**-**10**. The selectivity index (Si)/therapeutic index (Ti) are shown in brackets.

Cells/Comp.	HT-29	HCT-116	MiaPaCa-2	Panc-1	MRC-5	Zebrafish[a]
			IC_{50} (Si/Ti) [b]			LC_{50}
1	nd	**5.0 (6.8/48.9)**	**10.7 (3.2/22.8)**	nd	34	244.4
2	14.9	**10.3**	14.6	13. 3	12	68.9
3	49.5	27.7	20.3	20.1	>50	nd
4	38.7	**9.5** (2.4/**5.1**)	39.6	**10.1 (2.3/4.9)**	23	48.6
5	25	21.8	19.3	16.5	25.3	nd
6	11.6	**7.5** (1.6/**6.5**)	12	16.7	12.3	49.1
7	16.9	**4.9 (3.2/7)**	**9.2** (1.7/3.7)	**11** (1.4/**3.1**)	15.5	34.2
8	302.8	31.8	33.1	23.1	49.3	nd
9	173.2	22.1	21.8	16.4	>50	nd
10	32.9	21.5	21	20.1	>50	nd

nd = not determined. [a]The LC_{50} values have been determined in the zebrafish model only for the compounds with the IC_{50} values ≤ 11 μM. [b]Selectivity index (Si) is determined as the ratio between IC_{50} values on the normal and tumour cell lines; Therapeutic index (Ti) is determined as the ratio between corresponding LC_{50} and IC_{50} values. The most potent compounds showing the IC_{50} ≤ 11 μM and/or Si ≥ 3 and Ti ≥ 4 are bolded.

2.4 Solution behavior of complexes

Before performing the *in vivo* analysis (*vide infra*), we first studied the solution behavior of the complexes in an attempt to understand the observed differences in their anticancer activity. As mentioned previously [42], we hypothesize that the very promising complex **1** exerts its activity by alkylating (yet unknown) biological targets. We know that under conditions where the coordinated Br atom is not removed chemically (e.g. by addition of an Ag^+ salt) the complex shows limited reactivity (i.e. ligand exchange reaction) towards strong biological ligands such as the DNA bases guanine or adenine [42]. *fac*-$[Re(CO)_3]^+$ complexes show particular affinity for guanine [30, 37, 58, 59], and the base is the preferred ligand model in experiments aimed at understanding if DNA may be a target for such complexes [22, 35, 60]. In line with our current "alkylation hypothesis" the *in vitro* anticancer data reveal that only the compounds capable of diimine-based SN2 reactions (i.e. compounds **1**-**2** and **6**-**7**) show low anticancer μM IC_{50} values. Since the hydroxo derivatives (i.e. **3** and **8**) are inactive, we wondered if the hydrolysis rate of chloro and bromo compounds **1**-**2** and **6**-**7** might correlate to their activity *via* deactivation to the corresponding complexes **3** and **8**. Accordingly, we monitored via UV-visible spectroscopy the conversion depicted in Figure 3A. Table 3 presents the results of this analysis. We found that, with exception of complex **2**, the rate of hydrolysis of the species are very similar, and no clear correlation could be discerned with their corresponding IC_{50} values against HCT-116 and Panc-1 cells.

Next, we evaluated by ^{1}H-NMR spectroscopy the reaction of **1**-**2** and **6**-**7** with amino acid Boc-L-lysine (lys) as a model of biologically available amine groups (Figure 3B). Our initial experiments revealed a complex mixture of products, including species **3** and **8**, but also solvated derivatives of the different metal products (i.e. species ensuing from the exchange of the coordinated Br with S_1 and S_2 in Figure 3B). Thus, in order to unequivocally assign the NMR signals we first proceeded with synthesis of corresponding lys derivative (*o*-**11** and *m*-**11** in Figure 3B**,** where *o*- and *m*- stand for *ortho*- and *meta*- respectively). Under the specific experimental conditions, we found that compounds **1**, **2** and **6** all show very similar rates of reaction with lys (Table 3). Complex **7** was determined to be the most stable species showing limited and slower reactivity with the amino acid. In line with the UV-visible spectroscopy experiments, we did not find a correlation between corresponding IC_{50} values and the lys rate of reaction of the complexes.

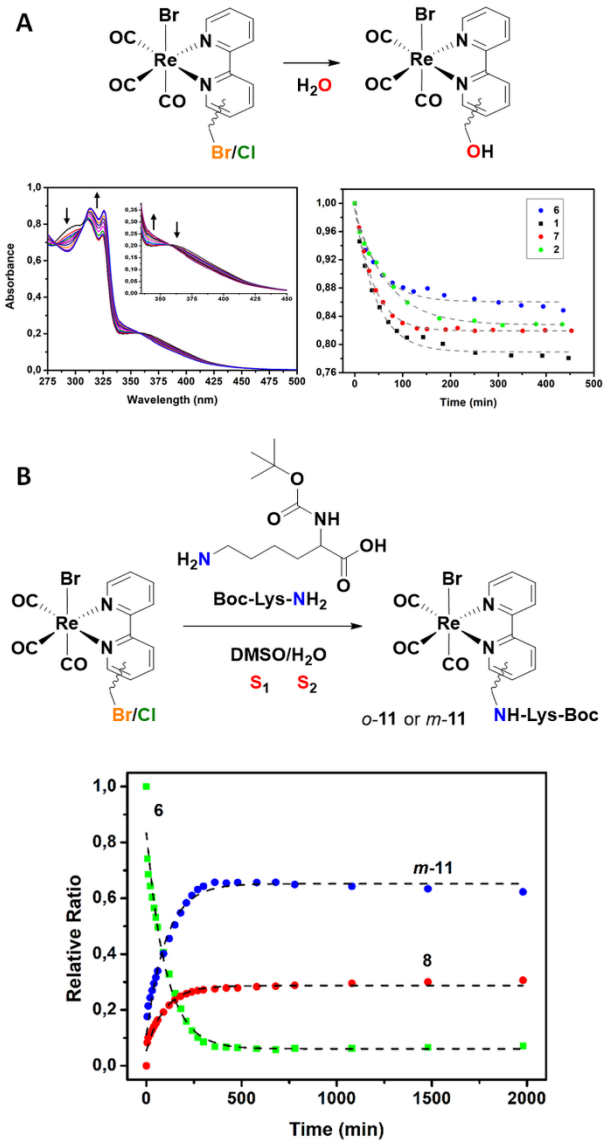

Figure 3. A: reaction depicting the hydrolysis of compounds **1**-**2** and **6**-**7** to the corresponding hydroxo complexes **3** and **8** (top), typical spectroscopic change observed during the reaction (bottom left) and plot of the time-dependent hydrolysis of compounds **1**-**2** and **6**-**7** according to visible spectroscopy data (bottom right). **B**: reaction of **1**-**2** and **6**-**7** with amino acid Boc-L-lysine (lys) as a model of biologically available amine groups giving the corresponding lys derivative *o*-**11** and *m*-**11** (top) and plot of a typical time-dependent speciation during the course of the reaction as observed by ^{1}H-NMR spectroscopy.

Table 3. Hydrolysis rate and initial lys rate of reaction of complexes **1**-**2** and **6**-**7**.

Complex	Hydrolysis rate[a] ($M\ s^{-1}$, 10^{-4})	Hydrolysis half life[a] ($t_{½}$, min)	Initial lys rate of rxn[b] ($M\ h^{-1}$, 10^{-3})	Concomitant hydrolysis rate during lys rxn[b] ($M\ h^{-1}$, 10^{-3})
1	1.35 ± 0.09	30.8 ± 2.0	3.92 ± 0.14	2.71 ± 0.24
2	0.89 ± 0.06	47.4 ± 3.2	4.82 ± 0.17	3.83 ± 0.25
6	1.24 ± 0.19	33.4 ± 3.8	3.39 ± 0.32	3.70 ± 0.38
7	1.56 ± 0.05	26.6 ± 1.0	0.96 ± 0.21	< 0.01

[a] By UV-Vis spectroscopy, in phosphate buffer, pH = 7.4, 25 °C. [b] By ^{1}H-NMR spectroscopy in 19:1 dimethyl sulfoxide-d6:D_2O, 37 °C. The reaction (rxn) refers to a 1 eq. Re complex : 2 eq. amino acid lys.

2.5 *In vivo* anticancer activity in the zebrafish xenograft models

The activity of complexes **2**, **4**, **6**, **7** and **9** was finally investigated *in vivo* against human pancreatic and colorectal carcinoma tumours using the zebrafish-Panc-1 and -HCT-116 xenograft models. Zebrafish xenografts are an established platform for translational research to human cancers, allowing the study of key hallmarks of cancer biology, such as tumour cells proliferation, dissemination, metastasis and angiogenesis [56, 61, 62]. Accordingly, in two separate experiments, Panc-1 and HCT-116 cells were fluorescently labelled and injected into the yolk of *Tg*(*fli1*:EGFP) and *Tg(-2.8fabp10a:*EGFP) embryos, respectively (Figures 4 and 5). At 3 days post injection (dpi), xenografts were processed for fluorescence microscopy in order to evaluate the effects of applied complexes on the tumour mass development and cancer cells dissemination and metastasis.

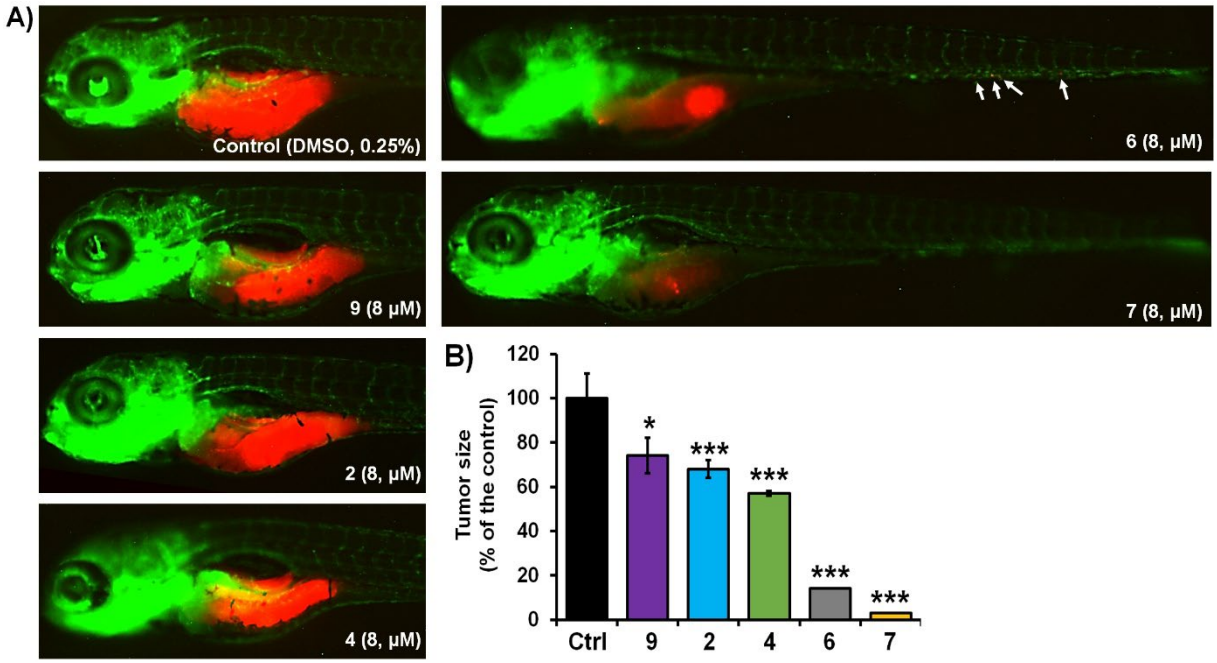

Figure 4. Anticancer activity of selected complexes against human Panc-1 cells in zebrafish xenografts. *Tg*(*fli1*:EGFP) xenografts (n = 20) were exposed to complexes at 8 μM doses, and then analysed after 3-days treatments for tumour progression and metastasis. Representative fluorescent microscopy images are shown (A); white solid arrows indicate disseminated cells. Only applied treatments of complexes **6** and **7** markedly reduced the tumour, growth compared to those in the control group (B). Data are normalized in relation to the control group (B). ∗P < 0.05; ∗∗P < 0.01; ∗∗∗P < 0.001.

Our results of zebrafish-Panc-1 xenografts (Figure 4) show that only treatments with **6** and **7** significantly inhibited pancreatic tumour growth *in vivo* ($P < 0.001$). Compound **7** was also effective in inhibiting cancer cells dissemination ($P < 0.001$). Both complexes were noticeably effective at an 8 μM concentration, lower than their respective *in vitro* IC_{50} values (Table 2). Comparison of tumour growth to untreated Panc-1 xenografts at 3 dpi (120 hpf) indicated that

6 and **7** reduced tumour mass in the treated xenografts by 86.0 ± 1.0 % and 97.5 ± 0.5 %, respectively ($P < 0.0001$, for both compounds). Compound **7** was also the most effective complex of the series in inhibiting colorectal tumour growth in zebrafish- HCT-116 xenografts (Figure 5). However, significant cancer growth inhibition was archived at 2 x *in vitro* IC_{50} value of the compound (i.e. at 10 μM). In zebrafish- HCT-116 xenografts, **6** showed much lower efficacy than in the pancreatic xenograft model (66.4 ± 11.1 % vs 86.1 ± 4.2 %, $P < 0.0001$). Finally, in the colorectal carcinoma model, compound **4** showed good inhibition of tumour growth (80.9 ± 7.3 %, $P < 0.0001$).

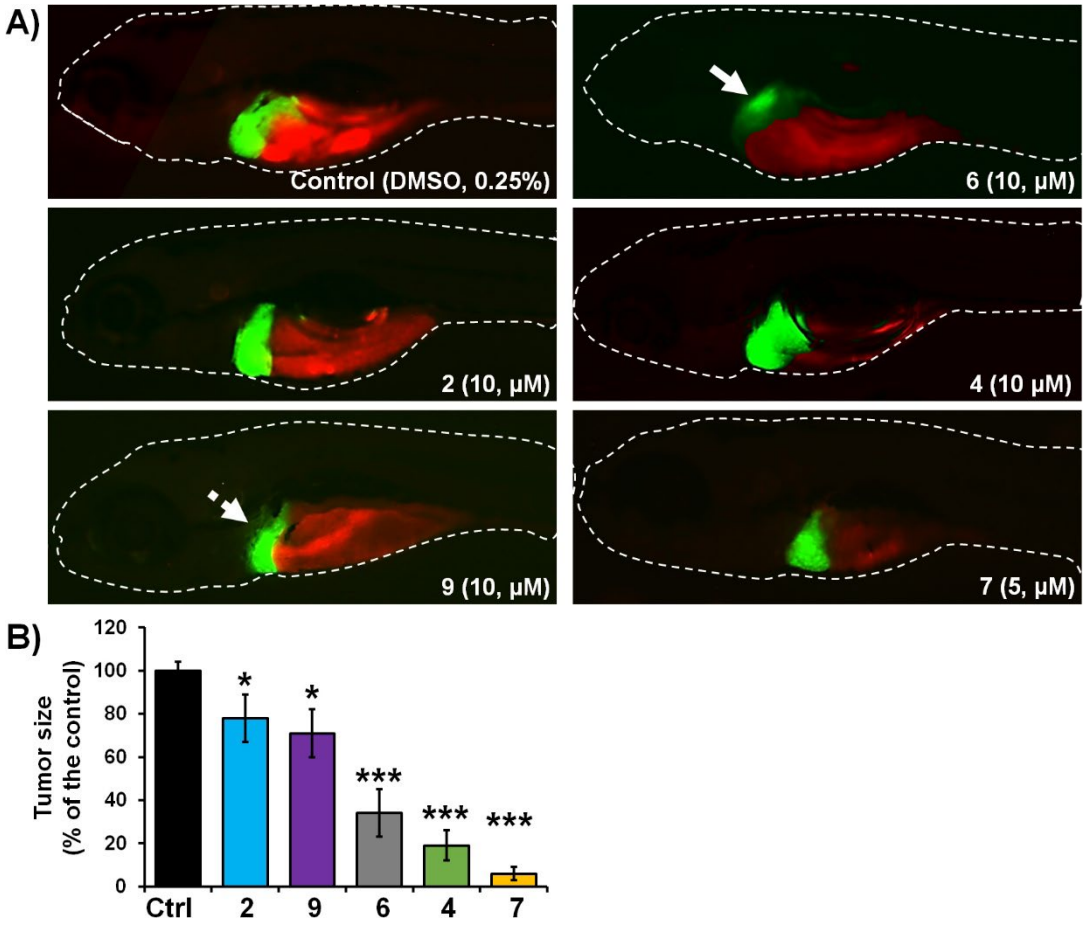

Figure 5. Anticancer activity of selected complexes against highly metastatic human HCT-116 cells in zebrafish xenografts. *Tg(-2.8fabp10a:*EGFP) xenografts (n = 20) were exposed to complexes at 10 μM doses, and then analysed after 3-day treatments for tumour progression and metastasis. Representative fluorescent microscopy images are shown (A); white solid arrow indicates treatment-affected liver (hepatotoxicity). Only applied treatments of complexes **4** and **7** markedly reduced the tumour growth, compared to those in the control group (B). Data are normalized in relation to the control group (B, C). ∗$P < 0.05$; ∗∗$P < 0.01$; ∗∗∗$P < 0.001$.

3. Conclusion

We have reported the synthesis, characterization, and *in vivo* evaluation of the anticancer activity of a series of 5- and 6-(halomethyl)-2,2'-bipyridine rhenium tricarbonyl complexes. On the basis of the initial identification of compound **1** [42], the study was initiated in order to understand if the presence and position of a reactive halomethyl substituent on the diimine ligand system of *fac*-$[Re(CO)_3]^+$ species may be a key structural or molecular feature for the design of active and non-toxic anticancer agents. Overall, our study revealed that, within the series of methyl-substituted diimine complexes, only compounds potentially able of ligand-based alkylating reactions (i.e. chloro- and bromomethyl complexes **2**, **6** and **7**) showed significant antiproliferative activity (as compared to the *unreactive* complexes, which are generally inactive). In terms of the relative potency of the species, we did not find a possible correlation with the hydrolysis rate or rate of reaction of the coordinated 5- and 6-(halomethyl)-2,2'-bipyridine with amino acid Boc-L-lysine (lys). Of the new species presented in this study, the data actually indicate that the most potent compound **7** is the least reactive. Thus, if our "alkylation hypothesis" holds true for **1**, the data seem to indicate that the possible mechanism of action of **7** may be different from that of **1**. In any case, it appears obvious to us that the same hypothesis cannot be generalized for this class of compounds. Nevertheless, compound **7** showed significant inhibition of pancreatic tumour growth *in vivo* in zebrafish-Panc-1 xenografts. The complex is noticeably effective at 8 μM concentration, lower than its *in vitro* IC_{50} values, and it is also effective in inhibiting cancer cells dissemination.

4. Experimental protocols

4.1. Materials and methods

All chemical reagents were purchased as reagent or analytical grade from commercial suppliers (Sigma-Aldrich, Alfa Aesar, TCI, Fluorochem) and used without further purification. Solvents were either used as received or dried over molecular sieves prior to use. ^1H and ^{13}C NMR spectra were recorded on a Bruker Avance III 500 MHz using residual solvent peaks as internal references. The following abbreviations are used: singlet (s), doublet (d), doublet of doublets (dd), triplet (t), doublet of triplets (td), quintuplet (quint), sextuplet (sext), and multiplet (m). HPLC analysis was performed on a Merck-Hitachi L7000. The analytical separations were conducted on a Machereye Nagel Nucleodur PolarTec column (5 μm particle size, 110 Å pore size, 250/3). The preparative separations were conducted on a Machereye Nagel Nucleodur C18 HTec column (5 μm particle size, 110 Å pore size, 250/21).

The flow rate was set to 0.5 mL/min for analytical separations and 5 mL/ min for the preparative ones. Eluting solvents and gradient are as previously described [63]. The eluting bands were detected at 250 nm. Analytical thin-layer chromatography (TLC) was performed on commercial silica plates (Merck 60-F 254, 0.25 mm thickness); compounds were visualized by UV light (254 nm and 366 nm). Preparative flash chromatography was performed with Merck silica gel (Si 60, 63-200 mesh). IR spectra were recorded on a PerkinElmer Spectrum 100 FT-IR spectrometer. The UV-Vis spectra were recorded on a Jasco V-730 and the emission on a spectrofluorometer FS5 (Edinburgh Instruments Ltd). Single crystal diffraction data collection was performed on a Stoe IPDS2 diffractometer (CuKα1 (λ = 1.5406 Å)) equipped with a cryostat from Oxford Cryosystems. The structures were solved with the ShelXT structure solution program using Intrinsic Phasing and refined with the ShelXL refinement package using Least Squares minimization [64, 65]. All crystal structures are deposited at the Cambridge Crystallographic Data Centre. CCDC numbers 2090791-2090797 contain the supplementary crystallographic data for this paper. These data can be obtained free of charge from the Cambridge Crystallographic Data Centre via www.ccdc.cam.ac.uk/structures.

4.2. Synthesis and characterization of ligands and complexes

4.2.1 General procedure for the preparation of ligands.

Preparation of 6-(difluoromethyl)-2,2'-bipyridine (L_5) and 5-(difluoromethyl)-2,2'-bipyridine (L_{10}): 2-bromo-6-(difluoromethyl)pyridine (**S_1**, or 2-bromo-5-(difluoromethyl)pyridine **S_2**, for **L_5** and **L_{10}** respectively, 1.0 equiv.) was added to a suspension of 2-(tributylstannyl)pyridine (**S_3**, 1.2 equiv.) in dry DMF. $Pd(PPh_3)_2(Cl)_2$ (cat.) was added under inert conditions, and then the reaction mixture was heated to 130 °C and stirred overnight. After completion of the reaction, the mixture was cooled to room temperature, and filtered over Celite. The residue was washed with DMF until the filtrate was colourless. The filtrate was evaporated and residue was dissolved in water. The solution was extracted 3 times with DCM, washed with brine, the combined organic phase was dried with $MgSO_4$ and then solvent was evaporated. The crude product was purified by flash column chromatography using DCM/MeOH 98:2 (v:v) to give a dark solid. This was dissolved in a small amount of diethyl ether followed by the addition of pentane. The solution was stirred overnight, then filtered and the residue washed with cold pentane. In order to increase the yield, the filtrate was evaporated and then precipitated again in pentane. The combined products were dried to give the desired compounds. Yields for L_5 and L_{10} were 17% and 38% respectively. **L_5**: ^{1}H NMR (400 MHz, $CDCl_3$) δ ppm 6.58 - 6.88 (m, 1 H), 7.35 (ddd, J = 7.46, 4.77, 1.22 Hz, 1 H), 7.67 (d, J = 7.70 Hz, 1 H), 7.85 (td, J = 7.76, 1.83 Hz, 1 H), 7.98 (t, J = 7.83 Hz, 1 H), 8.47 (dt, J = 7.95, 1.04 Hz, 1 H), 8.55 (dd, J = 7.95, 0.98 Hz, 1 H), 8.69 - 8.73 (m, 1 H). **L_{10}**: ^{1}H NMR (400 MHz, $CDCl_3$) δ ppm 6.62 - 6.94 (m, 1 H), 7.36 (ddd, J = 7.46, 4.77, 1.10 Hz, 1 H), 7.85 (td, J = 7.73, 1.77 Hz, 1 H), 7.97 (dt, J = 8.25, 0.95 Hz, 1 H), 8.45 (d, J = 7.95 Hz, 1 H), 8.53 (d, J = 8.19 Hz, 1 H), 8.71 (dd, J = 4.71, 0.67 Hz, 1 H), 8.81 (d, J = 0.73 Hz, 1 H).

Preparation of methyl [2,2'-bipyridine]-6-carboxylate (IM_1) and methyl [2,2'-bipyridine]-5-carboxylate (IM_2): The same procedure described above for the preparation of **L_5** and **L_{10}** was used starting with methyl 6-bromopicolinate (**S_4**, or methyl 6-bromonicotinate

S5, for **IM1** and **IM2** respectively, 1.0 equiv.) and S_3 (1.2 equiv.). Yields for IM_1 and IM_2 were 47% and 41% respectively. Analytical data are in agreement with data reported in literature for IM1 [66, 67] and IM2 [68].

Preparation of [2,2'-bipyridin]-6-ylmethanol (L_3) and [2,2'-bipyridin]-5-ylmethanol (L_8): Under argon, IM_1 (or IM_2, for **L3** and **L8** respectively, 1.0 equiv.) was dissolved in ethanol followed by the portion wise addition of $NaBH_4$ (3.0 equiv.). At the end of the addition, the reaction mixture was heated to 85 °C and stirred for 3h. After completion of the reaction, the solution was cooled down to room temperature and quenched by the addition of H_2O. The residual ethanol was evaporated, and the solution acidified by the addition of sulphuric acid and then washed 3 times with DCM. The aqueous phase was basified with NaOH 30% and extracted 3 times with DCM. The combined organic phase was then dried with $MgSO_4$. Evaporation of the solvent gave the pure products. Yields for **L3** and **L8** were 79% and 76% respectively. Analytical data are in agreement with data reported in literature for **L3** [69] and **L8** [70].

Preparation of 6-(bromomethyl)-2,2'-bipyridine (L_1) and 5-(bromomethyl)-2,2'-bipyridine (L_6): L_3 (or L_8, for **L1** and **L6** respectively, 1.0 equiv.) was dissolved in dry DCM under inert conditions while being cooled in an ice bath, followed by a slow addition of PBr_3 (3.0 equiv.). The ice bath was then removed, and the reaction mixture was stirred overnight at room temperature. After completion of the reaction, the solution was cooled again in an ice bath, and the reaction was quenched by the slow addition of cold water. Residual DCM was evaporated, and the residue was basified by the addition of NaOH 30%. For **L1**, the solution was filtered, and the residue was washed with cold water. For **L6**, the mixture was extracted 3 times with DCM, washed with water and dried with $MgSO_4$. The residual solvent was evaporated to give the desired product. Yields for **L1** and **L6** were 77% and 89% respectively. Analytical data are in agreement with data reported in literature for **L1** and **L6** [71].

Preparation of 6-(chloromethyl)-2,2'-bipyridine (L_2) and 5-(chloromethyl)-2,2'-bipyridine (L_7): L_3 (or L_8, for **L2** and **L7** respectively, 1.0 equiv.) was placed in a beaker and the solid was cooled in an ice bath before the dropwise addition of thionyl chloride (17.0 equiv.). Then the reaction mixture was heated to 80 °C and stirred for 2h. After completion of the reaction, the solution was cooled to room temperature and excess thionyl chloride was evaporated. The orange residue was then gently added to a saturated $NaHCO_3$ solution. The mixture was extracted 3 times with ethyl acetate, washed with brine, and dried with $MgSO_4$. The solvent was evaporated and the residue was purified by normal phase column chromatography using pentane/ethyl acetate 5:1 (v:v) to give the desired product. Yields for **L2** and **L7** were 83% and 80% respectively. Analytical data are in agreement with data reported in literature for **L7** [72] and **L2** [73].

4.2.2 General procedure for the preparation of *fac*-[Re(CO)$_3$(L$_\#$)Br] complexes 1-10

Bromopentacarbonylrhenium(I) (1.0 equiv.) was dissolved in hot toluene (60 °C) under argon. The diimine ligand (1.0 equiv.) was added, and the solution was refluxed overnight at 85-95 °C. The reaction mixture was cooled to room temperature, and then placed in the fridge for 1

h. The formed precipitate was filtered off, washed with cold toluene, and dried in vacuo. Generally, no further purification was necessary to give the pure products described below.

***fac*-[Re(CO)$_3$(L$_2$)Br] (2)**. Yellow powder, yield 96%. ESI-MS analysis (positive mode) m/z= 474.9 $[C_{14}H_9BrClN_2O_3Re]^+$. IR (solid, νCO cm^{-1}): 2015.43, 1882.86. UV-Vis ($CHCl_3$, nm): 301, 372. ^{1}H NMR (400 MHz, acetonitrile-d3) δ ppm 5.11 - 5.23 (m, 2 H) 7.65 (ddd, J=7.64, 5.56, 1.10 Hz, 1 H) 7.89 - 8.01 (m, 1 H) 8.14 - 8.28 (m, 2 H) 8.35 - 8.49 (m, 2 H) 9.06 - 9.15 (m, 1 H). ^{13}C NMR (126 MHz, acetonitrile-d_3) δ ppm 48.64 - 51.40 (m, 1 C) 123.48 - 126.23 (m, 3 C) 126.65 - 128.85 (m, 2 C) 139.05 - 142.77 (m, 3 C) 153.49 (d, J=4.54 Hz, 2 C). Crystals suitable for X-ray diffraction were obtained from layering of hexane on DCM.

***fac*-[Re(CO)$_3$(L$_3$)Br] (3)**. Yellow powder, yield 96%. ESI-MS analysis (positive mode) m/z= 456.9 $[C_{14}H_{10}BrN_2O_4Re]^+$. IR (solid, νCO cm^{-1}): 2015.70, 1919.28, 1889.42. UV-Vis ($CHCl_3$, nm): 299.5, 367.5. ^{1}H NMR (500 MHz, DMSO-d6) δ ppm 4.81 - 4.96 (m, 2 H) 6.20 (br. s., 1 H) 7.72 - 7.78 (m, 1 H) 8.00 (d, J=7.93 Hz, 1 H) 8.28 - 8.37 (m, 2 H) 8.65 (d, J=7.93 Hz, 1 H) 8.76 (d, J=8.24 Hz, 1 H) 9.07 (d, J=5.34 Hz, 1 H). ^{13}CNMR (126 MHz, DMSO-d_6) δ ppm 67.53 (s, 1 C) 122.55 (s, 1 C) 123.87 (s, 1 C) 124.55 (s, 1 C) 127.74 (s, 1 C) 140.49 (d, J=14.53 Hz, 1 C) 152.77 (s, 1 C) 155.53 (s, 1 C) 156.14 (s, 1 C) 164.80 (s, 1 C) 188.44 (s, 1 C) 197.05 (s, 1 C). Crystals suitable for X-ray diffraction were obtained from layering of hexane on DCM.

***fac*-[Re(CO)$_3$(L$_4$)Br] (4)**. Yellow powder, yield 91%. ESI-MS analysis (positive mode) m/z= 440.9 $[C_{14}H_{10}BrN_2O_3Re]^+$. IR (solid, νCO cm^{-1}): 2017.70, 1896.71. UV-Vis ($CHCl_3$, nm): 299, 369. ^{1}H NMR (400 MHz, acetonitrile-d3) δ ppm 3.01 (s, 3 H) 7.57 - 7.69 (m, 2 H) 8.04 (t, J=7.89 Hz, 1 H) 8.12 - 8.20 (m, 1 H) 8.26 (d, J=7.95 Hz, 1 H) 8.35 - 8.41 (m, 1 H) 9.04 - 9.12 (m, 1 H). ^{13}C NMR (126 MHz, DMSO-d6) d ppm 17.67 (s, 1 C) 123.73 (d, J=17.26 Hz, 1 C) 127.29 (s, 1 C) 138.26 (s, 1 C) 139.20 - 141.08 (m, 2 C) 151.49 - 153.45 (m, 2 C) 155.21 (s, 1 C).

***fac*-[Re(CO)$_3$(L$_5$)Br] (5)**. Yellow powder, yield 95%. ESI-MS analysis (positive mode) m/z= 476.9 $[C_{14}H_8BrF_2N_2O_3Re]^+$. IR (solid, νCO cm^{-1}): 2017.49 1889.73. UV-Vis ($CHCl_3$, nm): 296, 377. ^{1}H NMR (500 MHz, DMSO-d6) δ ppm 7.17 - 7.42 (m, 1 H) 7.80 (t, J=6.41 Hz, 1 H) 7.91 (d, J=5.65 Hz, 1 H) 8.35 (t, J=7.86 Hz, 1 H) 8.91 (d, J=8.09 Hz, 1 H) 8.94 (s, 1 H) 9.07 (s, 1 H) 9.20 (d, J=5.65 Hz, 1 H). ^{13}C NMR (126 MHz, DMSO-d_6) d ppm 110.58 (s, 1 C) 112.49 (s, 1 C) 114.40 (s, 1 C) 120.43 - 121.34 (m, 1 C) 123.03 - 124.59 (m, 1 C) 124.84 (s, 1 C) 128.18 (s, 1 C) 140.19 (s, 1 C) 143.85 - 145.74 (m, 1 C) 153.07 (s, 1 C) 153.67 - 154.97 (m, 1 C) 156.26 (s, 1 C) 188.91 (s, 1 C) 196.99 (d, J=16.35 Hz, 1 C). Crystals suitable for X-ray diffraction were obtained from layering of hexane on DCM.

***fac*-[Re(CO)$_3$(L$_6$)Br] (6)**. Yellow powder, yield 68%. ESI-MS analysis (positive mode) m/z= 519.1 $[C_{14}H_9Br_2N_2O_3Re]^+$. IR (solid, νCO cm^{-1}): 2016.66, 1882.55. UV-Vis ($CHCl_3$, nm): 298, 384. ^{1}H NMR (500 MHz, DMSO-d6) δ ppm 4.96 (s, 2 H) 7.71 - 7.80 (m, 1 H) 8.33 (t, J=7.86 Hz, 1 H) 8.40 (d, J=8.39 Hz, 1 H) 8.76 (t, J=8.70 Hz, 2 H) 9.04 (d, J=5.34 Hz, 1 H) 9.12 (s, 1 H). ^{13}C NMR (126 MHz, $CDCl_3$-d) δ ppm 14.04 (s, 2 C) 22.33 (s, 1 C) 27.04 (s, 1 C) 34.12 (s, 1 C) 54.55 (s, 1 C) 121.76 - 124.24 (m, 1 C) 127.25 (s, 1 C) 136.74 - 140.99 (m, 2 C) 151.71 - 156.38 (m, 1 C). Crystals suitable for X-ray diffraction were obtained from layering of pentane on chloroform.

***fac*-[Re(CO)$_3$(L$_7$)Br] (7**). Yellow powder, yield 81%. ESI-MS analysis (positive mode) m/z= 474.9 [$C_{14}H_9BrClN_2O_3Re$]$^+$. IR (solid, νCO cm^{-1}): 2017.48, 1882.97. UV-Vis ($CHCl_3$, nm): 296, 276. ^{1}H NMR (500 MHz, DMSO-d6) δ ppm 5.05 (s, 2 H) 7.77 (br. s., 1 H) 8.34 (s, 1 H) 8.41 (d, J=7.17 Hz, 1 H) 8.79 (dd, J=15.87, 8.24 Hz, 2 H) 9.05 (d, J=5.49 Hz, 1 H) 9.12 (s, 1 H). ^{13}C NMR (126 MHz, DMSO-d6) δ ppm 41.53 (s, 1 C) 123.27 - 125.47 (m, 2 C) 127.97 (s, 1 C) 137.83 (s, 1 C) 139.26 - 141.18 (m, 2 C) 150.56 - 154.00 (m, 2 C) 154.00 - 155.79 (m, 2 C) 189.29 (s, 1 C) 195.62 - 197.55 (m, 2 C). Crystals suitable for X-ray diffraction were obtained from layering of hexane on DCM.

***fac*-[Re(CO)$_3$(L$_8$)Br] (8**). Yellow powder, yield 68%. ESI-MS analysis (positive mode) m/z= 465.9 [$C_{14}H_{10}BrN_2O_4Re$]$^+$. IR (solid, νCO cm^{-1}): 2016.90, 1869.77. UV-Vis ($CHCl_3$, nm): 294, 371. ^{1}H NMR (500 MHz, DMSO-d6) δ ppm 4.74 (d, J=5.65 Hz, 2 H) 5.73 (t, J=5.72 Hz, 1 H) 7.71 - 7.77 (m, 1 H) 8.22 (d, J=8.24 Hz, 1 H) 8.32 (t, J=7.86 Hz, 1 H) 8.73 (d, J=8.39 Hz, 2 H) 8.96 (s, 1 H) 9.02 (d, J=5.49 Hz, 1 H) . ^{13}C NMR (126 MHz, DMSO-d6) δ ppm 59.69 (s, 1 C) 122.58 - 124.92 (m, 2 C) 127.58 (s, 1 C) 137.89 (s, 1 C) 140.18 (s, 1 C) 142.51 (s, 1 C) 150.48 (s, 1 C) 152.35 - 154.28 (m, 2 C) 155.16 (s, 1 C) 189.45 (s, 1 C) 197.38 (s, 1 C) 201.66 (s, 1 C).

***fac*-[Re(CO)$_3$(L$_9$)Br] (9**). Yellow powder, yield 74%. ESI-MS analysis (positive mode) m/z= 440.9 [$C_{14}H_{10}BrN_2O_3Re$]$^+$. IR (solid, νCO cm^{-1}): 2017.70, 1896.71. UV-Vis ($CHCl_3$, nm): 295, 368. ^{1}H NMR (500 MHz, DMSO-d6) δ ppm 2.50 (s, 3 H) 7.68 - 7.76 (m, 1 H) 8.16 (d, J=8.39 Hz, 1 H) 8.30 (t, J=7.86 Hz, 1 H) 8.62 - 8.73 (m, 2 H) 8.86 (s, 1 H) 9.01 (d, J=5.34 Hz, 1 H). ^{13}C NMR (126 MHz, DMSO-d_6) d ppm 17.67 (s, 1 C) 123.79 (s, 2 C) 127.29 (s, 1 C) 138.26 (s, 1 C) 140.00 (s, 1 C) 140.51 (s, 1 C) 151.94 - 153.15 (m, 2 C) 155.21 (s, 1 C) 189.41 (s, 1 C) 197.12 (s, 2 C) 206.33 (s, 1 C). Crystals suitable for X-ray diffraction were obtained from layering of pentane on DCM.

***fac*-[Re(CO)$_3$(L$_{10}$)Br] (10)**. Yellow powder, yield 71%. ESI-MS analysis (positive mode) m/z= 467.9 [$C_{14}H_8BrF_2N_2O_3Re$]$^+$. IR (solid, νCO cm^{-1}): 2020.67, 1887.81. UV-Vis ($CHCl_3$, nm): 295, 378. ^{1}H NMR (500 MHz, DMSO-d_6) δ ppm 7.26 - 7.51 (m, 1 H) 7.82 (t, J=6.56 Hz, 1 H) 8.37 (t, J=7.86 Hz, 1 H) 8.57 (d, J=8.55 Hz, 1 H) 8.82 - 8.94 (m, 2 H) 9.08 (d, J=5.34 Hz, 1 H) 9.19 (s, 1 H). 13C NMR (126 MHz, DMSO-d6) d ppm 20.89 (s, 1 C) 110.28 (s, 1 C) 112.17 (s, 1 C) 114.07 (s, 1 C) 122.35 - 126.48 (m, 2 C) 127.17 - 129.93 (m, 2 C) 140.24 (s, 1 C) 150.39 (t, J=7.72 Hz, 1 C) 153.17 (s, 2 C) 188.90 (s, 1 C) 196.87 (d, J=18.17 Hz, 1 C). Crystals suitable for X-ray diffraction were obtained from layering of hexane on DCM.

Preparation of Boc-L-lysine *fac*-[Re(CO)$_3$(L-lys)Br] deriatives *o*-11 and *m*-11.

***fac*-[Re(CO)$_3$(L-*o*-lys)Br] (*o*-11).** Compound **1** (25 mg, 0.04 mmol) was dissolved in dry acetonitrile (3 mL) and the solution was purged with argon for 10 minutes, before the addition of N,N-diisopropylethylamine (DIPEA, 26 μL, 0.15 mmol). After 20 minutes, a degassed solution of Boc-L-Lysine (29 mg, 0.12 mmol) in 2 mL H_2O/Acetonitrile (3/1 v/v) was added to the reaction mixture under inert conditions and it was stirred over night at room temperature. The solvent was evaporated and the residual product was dissolved in ethyl acetate, washed 2 times with water and brine and dried with $NaSO_4$. The organic phase was evaporated, the crude product was dissolved in a minimal amount of DCM and then precipitated by the addition of 30 mL hexane. After placing the solution in the fridge overnight, the same was filtered to give a yellow solid. The filtrate was reduced and again hexane was added to give more of the crude product. The product was then dissolved in

methanol, purified by HPLC and lyophilized to give the desired product as a light yellow powder. Yield 16 mg, 0.023 mmol, 56 %. ESI-MS analysis (positive mode) m/z = 684.8 $[C_{25}H_{30}N_4O_7Re]^+$. IR (solid, νCO cm^{-1}): 2016.26, 1882.24. UV-Vis ($CHCl_3$, nm): 302, 324, 350. ^{1}H NMR (500 MHz, DMSO-d6) δ ppm 1.15 (d, J=12.97 Hz, 2 H) 1.22 - 1.37 (m, 11 H) 1.58 (br. s., 2 H) 2.03 - 2.22 (m, 2 H) 3.56 (br. s., 1 H) 4.02 (d, J=13.89 Hz, 1 H) 4.40 (d, J=14.19 Hz, 1 H) 7.71 - 7.83 (m, 1 H) 7.88 (d, J=7.63 Hz, 1 H) 8.24 - 8.38 (m, 2 H) 8.63 - 8.79 (m, 2 H) 9.01 (d, J=5.34 Hz, 1 H).

***fac*-[Re(CO)$_3$(L-*m*-lys)Br] (*m*-11).** The same procedure for the synthesis of ***o*-11** was applied but starting with compound **6**. Yield 8 mg, 0.013 mmol, 28 %. ESI-MS analysis (positive mode) m/z = 684.8 $[C_{25}H_{30}N_4O_7Re]^+$. IR (solid, νCO cm^{-1}): 2018.11, 1882.36. ^{1}H NMR (500 MHz, DMSO-d6) δ ppm 0.70 - 0.92 (m, 2 H) 1.00 - 1.15 (m, 4 H) 1.18 - 1.41 (m, 11 H) 2.20 - 2.37 (m, 1 H) 3.86 (d, J=17.40 Hz, 2 H) 7.74 (br. s., 1 H) 8.10 - 8.25 (m, 1 H) 8.27 - 8.43 (m, 1 H) 8.62 - 8.81 (m, 2 H) 8.89 - 9.09 (m, 2 H).

4.3 Cytotoxicity evaluation

Antiproliferative activity of the compounds was tested in a panel against tumour cells lines HCT-116 (colorectal carcinoma cells), HT-29 (colorectal adenocarcinoma cells) Mia PaCa-2 (pancreatic carcinoma cells) and Panc-1 (epithelial pancreatic carcinoma cells), as well as on normal human lung fibroblasts (MRC-5), all from ATCC collection. Compounds were freshly dissolved in DMSO and used for the bioactivity assessments. Cytotoxicity in terms of antiproliferative effects was tested by the standard 3-(4,5-dimethylthiazol-2-yl)-2,5-diphenyltetrazolium bromide (MTT) assay [74]. The assay was carried out as previously described [42].

4.4 *In vivo* toxicity assessment

Toxicity evaluation of the complexes was carried in the zebrafish (Danio rerio) model according to the general rules of the OECD Guidelines for the Testing of Chemicals (OECD, 2013, Test No. 236) [75]. All experiments involving zebrafish were performed in compliance with the European directive 2010/63/EU and the ethical guidelines of the Guide for Care and Use of Laboratory Animals of the Institute of Molecular Genetics and Genetic Engineering, University of Belgrade. Wild type (AB) zebrafish were kindly provided by Dr. Ana Cvejić (Wellcome Trust Sanger Institute, Cambridge, UK). Experiments were performed as previously reported [42].

4.5 Anticancer activity evaluation in human CRC-zebrafish xenografts

Cancer cells were cultured in RPMI-1640 supplemented with 10 % FBS, 100 μg/mL streptomycin and 100 UmL^{-1} penicillin, and grown as a monolayer in humidified atmosphere

of 95% air and 5% CO_2 at 37 °C. Prior to microinjection, the cells were washed once with PBS and trypsinized (0.25% trypsin/0.53 mM EDTA) to obtain a single cell suspension. After centrifugation at 1200 rpm for 5 min, the cells were resuspended in serum-free RPMI medium and labelled with 2 μM CellTracker^{TM} RedCMTPX (Thermofisher Scientific) according to the manufacturer's instructions.

4.6 Zebrafish xenografts injection and Treatment.

The zebrafish xenografts with human HCT-116 cells were established according to the previously described procedure [76]. Before the microinjections, Tg(fli1:EGFP) and *Tg*(-*2.8fabp10a*:EGFP) embryos were kept at 28 °C and manually dechorionated few hours before the injection. At 48 hpf, 5 nL of cells suspension containing 150 labelled cells was microinjected into the yolk of anesthetized embryos by a pneumatic picopump (PV820, World Precision Instruments, USA). Exact number of cells was confirmed by dispensing the injected volume onto a microscope slide and by visual counting. After injection, embryos were incubated to recover for at least one hour at 28 °C, dead embryos were removed, and alive embryos were transferred into 24-well plates containing 1 mL of embryo water and 10 embryos per well. The injected xenografts were treated with different doses of complex **1** and **4** (1/2, 1/4 and 1/8 of IC_{50} values), and maintained at 33 °C by 120 hpf. DMSO (0.25%) was used as a negative control. The survival and development of the xenografted embryos was recorded every day until the end of experiment. At 3 days post injection (dpi), anesthetized xenografts were processed by fluorescent microscopy. The tumour size was determined by the fluorescent images using ImageJ programme. The experiment was repeated two times.

4.7 Statistical analysis.

The experimental results were expressed as mean values ± SD. The differences in anti-angiogenic phenotypes between the untreated and treated groups were determined according to χ^2 test. In other tests, the differences between the untreated and treated groups, as well as between the treatments were evaluated using the one-way ANOVA followed by a comparison of the means by Bonferroni test (P = 0.05). All analyses were performed using SPSS 20 (SPSS Inc., Chicago, IL) software package.

Funding

Financial support from the Swiss National Science Foundation (project# 200021_196967, K.S. and F. Z.), the University of Fribourg and the Institute of Molecular Genetics and

Genetic Engineering from the University of Belgrade (Ministry of Education, Science and Technological Development of the Republic of Serbia, 451-03-68/2022-14/200042) are gratefully acknowledged.

Declaration of competing interest

The authors declare that they have no known competing financial interests or personal relationships that could have appeared to influence the work reported in this paper.

References

[1] S. Ghosh, Cisplatin: The first metal based anticancer drug, Bioorg. Chem., 88 (2019) 102925.
[2] S. Su, Y. Chen, P. Zhang, R. Ma, W. Zhang, J. Liu, T. Li, H. Niu, Y. Cao, B. Hu, J. Gao, H. Sun, D. Fang, J. Wang, P.G. Wang, S. Xie, C. Wang, J. Ma, The role of Platinum(IV)-based antitumor drugs and the anticancer immune response in medicinal inorganic chemistry. A systematic review from 2017 to 2022, Eur. J. Med. Chem., 243 (2022) 114680.
[3] S. Sen, M. Won, M.S. Levine, Y. Noh, A.C. Sedgwick, J.S. Kim, J.L. Sessler, J.F. Arambula, Metal-based anticancer agents as immunogenic cell death inducers: the past, present, and future, Chem. Soc. Rev., 51 (2022) 1212-1233.
[4] R. Paprocka, M. Wiese-Szadkowska, S. Janciauskiene, T. Kosmalski, M. Kulik, A. Helmin-Basa, Latest developments in metal complexes as anticancer agents, Coord. Chem. Rev., 452 (2022) 214307.
[5] Z.-Y. Li, Q.-H. Shen, Z.-W. Mao, C.-P. Tan, Rising Interest in the Development of Metal Complexes in Cancer Immunotherapy, Chem. Asian J., 17 (2022) e202200270.
[6] K. Schindler, F. Zobi, Anticancer and Antibiotic Rhenium Tri- and Dicarbonyl Complexes: Current Research and Future Perspectives, Molecules, 27 (2022) 539.
[7] Z. Huang, J.J. Wilson, Therapeutic and Diagnostic Applications of Multimetallic Rhenium(I) Tricarbonyl Complexes, Eur. J. Inorg. Chem. , 2021 (2021) 1312-1324.
[8] M. Mkhatshwa, J.M. Moremi, K. Makgopa, A.-L.E. Manicum, Nanoparticles Functionalised with Re(I) Tricarbonyl Complexes for Cancer Theranostics, Int. J. Mol. Sci., 22 (2021) 6546.
[9] H.S. Liew, C.-W. Mai, M. Zulkefeli, T. Madheswaran, L.V. Kiew, N. Delsuc, M.L. Low, Recent Emergence of Rhenium(I) Tricarbonyl Complexes as Photosensitisers for Cancer Therapy, Molecules, 25 (2020) 4176.
[10] P. Collery, D. Desmaele, V. Vijaykumar, Design of Rhenium Compounds in Targeted Anticancer Therapeutics, Curr. Pharm. Des., 25 (2019) 1-17.
[11] E.B. Bauer, A.A. Haase, R.M. Reich, D.C. Crans, F.E. Kühn, Organometallic and coordination rhenium compounds and their potential in cancer therapy, Coord. Chem. Rev., 393 (2019) 79-117.
[12] C.C. Konkankit, S.C. Marker, K.M. Knopf, J.J. Wilson, Anticancer activity of complexes of the third row transition metals, rhenium, osmium, and iridium, Dalton Trans., 47 (2018) 9934-9974.
[13] L.C. Lee, K.K. Leung, K.K. Lo, Recent development of luminescent rhenium(I) tricarbonyl polypyridine complexes as cellular imaging reagents, anticancer drugs, and antibacterial agents, Dalton Trans., 46 (2017) 16357-16380.
[14] A. Leonidova, G. Gasser, Underestimated Potential of Organometallic Rhenium Complexes as Anticancer Agents, ACS Chem. Biol., 9 (2014) 2180-2193.
[15] A. Sharma S, V. N, B. Kar, U. Das, P. Paira, Target-specific mononuclear and binuclear rhenium(i) tricarbonyl complexes as upcoming anticancer drugs, RSC Adv., 12 (2022) 20264-20295.
[16] A.J. Amoroso, M.P. Coogan, J.E. Dunne, V. Fernández-Moreira, J.B. Hess, A.J. Hayes, D. Lloyd, C. Millet, S.J.A. Pope, C. Williams, Rhenium fac tricarbonyl bisimine complexes: biologically useful fluorochromes for cell imaging applications, Chem. Commun., (2007) 3066-3068.
[17] M.-W. Louie, M. Ho-Chuen Lam, K. Kam-Wing Lo, Luminescent Polypyridinerhenium(I) Bis-Biotin Complexes as Crosslinkers for Avidin, Eur. J. Inorg. Chem., 2009 (2009) 4265-4273.
[18] A. Leonidova, V. Pierroz, L.A. Adams, N. Barlow, S. Ferrari, B. Graham, G. Gasser, Enhanced Cytotoxicity through Conjugation of a "Clickable" Luminescent Re(I) Complex to a Cell-Penetrating Lipopeptide, ACS Med. Chem. Lett., 5 (2014) 809-814.
[19] R.R. Ye, C.P. Tan, M.H. Chen, L. Hao, L.N. Ji, Z.W. Mao, Mono- and Dinuclear Phosphorescent Rhenium(I) Complexes: Impact of Subcellular Localization on Anticancer Mechanisms, Chem. Eur. J., 22 (2016) 7800-7809.
[20] S. Clede, F. Lambert, R. Saint-Fort, M.A. Plamont, H. Bertrand, A. Vessieres, C. Policar, Influence of the Side-Chain Length on the Cellular Uptake and the Cytotoxicity of Rhenium Triscarbonyl

Derivatives: A Bimodal Infrared and Luminescence Quantitative Study, Chem. Eur. J., 20 (2014) 8714-8722.
[21] I. Kitanovic, S.Z. Can, H. Alborzinia, A. Kitanovic, V. Pierroz, A. Leonidova, A. Pinto, B. Spingler, S. Ferrari, R. Molteni, A. Steffen, N. Metzler-Nolte, S. Wolfl, G. Gasser, A Deadly Organometallic Luminescent Probe: Anticancer Activity of a ReI Bisquinoline Complex, Chem. Eur. J., 20 (2014) 2496-2507.
[22] K.M. Knopf, B.L. Murphy, S.N. MacMillan, J.M. Baskin, M.P. Barr, E. Boros, J.J. Wilson, In Vitro Anticancer Activity and in Vivo Biodistribution of Rhenium(I) Tricarbonyl Aqua Complexes, J. Am. Chem. Soc., 139 (2017) 14302-14314.
[23] M. König, D. Siegmund, L.J. Raszeja, A. Prokop, N. Metzler-Nolte, Resistance-breaking profiling and gene expression analysis on an organometallic ReI–phenanthridine complex reveal parallel activation of two apoptotic pathways, Med. Chem. Commun., 9 (2018) 173-180.
[24] C.C. Konkankit, A.P. King, K.M. Knopf, T.L. Southard, J.J. Wilson, In Vivo Anticancer Activity of a Rhenium(I) Tricarbonyl Complex, ACS Med. Chem. Lett., 10 (2019) 822-827.
[25] F.X. Wang, J.H. Liang, H. Zhang, Z.H. Wang, Q. Wan, C.P. Tan, L.N. Ji, Z.W. Mao, Mitochondria-Accumulating Rhenium(I) Tricarbonyl Complexes Induce Cell Death via Irreversible Oxidative Stress and Glutathione Metabolism Disturbance, ACS Appl. Mater. Interfaces, 11 (2019) 13123-13133.
[26] M. Munoz-Osses, F. Godoy, A. Fierro, A. Gomez, N. Metzler-Nolte, New organometallic imines of rhenium(I) as potential ligands of GSK-3 beta: synthesis, characterization and biological studies, Dalton Trans., 47 (2018) 1233-1242.
[27] C.-C. Pagoni, V.-S. Xylouri, G.C. Kaiafas, M. Lazou, G. Bompola, E. Tsoukas, L.C. Papadopoulou, G. Psomas, D. Papagiannopoulou, Organometallic rhenium tricarbonyl–enrofloxacin and –levofloxacin complexes: synthesis, albumin-binding, DNA-interaction and cell viability studies, J. Biol. Inorg. Chem., 24 (2019) 609-619.
[28] M. Kaplanis, G. Stamatakis, V.D. Papakonstantinou, M. Paravatou-Petsotas, C.A. Demopoulos, C.A. Mitsopoulou, Re(I) tricarbonyl complex of 1,10-phenanthroline-5,6-dione: DNA binding, cytotoxicity, anti-inflammatory, and anti-coagulant effects towards platelet activating factor, J. Inorg. Biochem., 135 (2014) 1-9.
[29] G. Balakrishnan, T. Rajendran, K. Senthil Murugan, M. Sathish Kumar, V.K. Sivasubramanian, M. Ganesan, A. Mahesh, T. Thirunalasundari, S. Rajagopal, Interaction of rhenium(I) complex carrying long alkyl chain with Calf Thymus DNA: Cytotoxic and cell imaging studies, Inorg. Chim. Acta, 434 (2015) 51-59.
[30] F. Zobi, B. Spingler, R. Alberto, Guanine and plasmid DNA binding of mono- and trinuclear fac-[Re(CO)(3)](+) complexes with amino acid Ligands, Chembiochem, 6 (2005) 1397-1405.
[31] A.P. King, S.C. Marker, R.V. Swanda, J.J. Woods, S.-B. Qian, J.J. Wilson, A Rhenium Isonitrile Complex Induces Unfolded Protein Response-Mediated Apoptosis in Cancer Cells, Chem. Eur. J., 25 (2019) 9206-9210.
[32] C.C. Konkankit, J. Lovett, H.H. Harris, J.J. Wilson, X-Ray fluorescence microscopy reveals that rhenium(i) tricarbonyl isonitrile complexes remain intact in vitro, Chem. Commun., 56 (2020) 6515-6518.
[33] S.C. Marker, A.P. King, S. Granja, B. Vaughn, J.J. Woods, E. Boros, J.J. Wilson, Exploring the In Vivo and In Vitro Anticancer Activity of Rhenium Isonitrile Complexes, Inorg. Chem., 59 (2020) 10285-10303.
[34] P. Collery, G. Bastian, F. Santoni, A. Mohsen, M. Wei, T. Collery, A. Tomas, D. Desmaele, J. D'Angelo, Uptake and efflux of rhenium in cells exposed to rhenium diseleno-ether and tissue distribution of rhenium and selenium after rhenium diseleno-ether treatment in mice, Anticancer Res., 34 (2014) 1679-1689.
[35] P. Collery, A. Mohsen, A. Kermagoret, S. Corre, G. Bastian, A. Tomas, M. Wei, F. Santoni, N. Guerra, D. Desmaele, J. d'Angelo, Antitumor activity of a rhenium (I)-diselenoether complex in experimental models of human breast cancer, Invest. New Drugs, 33 (2015) 848-860.

[36] V. Veena, A. Harikrishnan, B. Lakshmi, S. Khanna, D. Desmaele, P. Collery, A New Model Applied for Evaluating a Rhenium-diselenium Drug: Breast Cancer Cells Stimulated by Cytokines Induced from Polynuclear Cells by LPS, Anticancer Res., 40 (2020) 1915-1920.
[37] P. Collery, V. Veena, A. Harikrishnan, D. Desmaele, The rhenium(I)-diselenoether anticancer drug targets ROS, TGF-β1, VEGF-A, and IGF-1 in an in vitro experimental model of triple-negative breast cancers, Invest. New Drugs, 37 (2019) 973-983.
[38] P.V. Simpson, I. Casari, S. Paternoster, B.W. Skelton, M. Falasca, M. Massi, Defining the Anti-Cancer Activity of Tricarbonyl Rhenium Complexes: Induction of G2/M Cell Cycle Arrest and Blockade of Aurora-A Kinase Phosphorylation, Chem. Eur. J., 23 (2017) 6518-6521.
[39] A. Domenichini, I. Casari, P.V. Simpson, N.M. Desai, L. Chen, C. Dustin, J.S. Edmands, A. van der Vliet, M. Mohammadi, M. Massi, M. Falasca, Rhenium N-heterocyclic carbene complexes block growth of aggressive cancers by inhibiting FGFR- and SRC-mediated signalling, J. Exp. Clin. Cancer Res., 39 (2020) 276.
[40] S.N. Sovari, N. Radakovic, P. Roch, A. Crochet, A. Pavic, F. Zobi, Combatting AMR: A molecular approach to the discovery of potent and non-toxic rhenium complexes active against C. albicans-MRSA co-infection, Eur. J. Med. Chem., 226 (2021) 113858.
[41] J. Rossier, D. Hauser, E. Kottelat, B. Rothen-Rutishauser, F. Zobi, Organometallic cobalamin anticancer derivatives for targeted prodrug delivery via transcobalamin-mediated uptake, Dalton Trans., 46 (2017) 2159-2164.
[42] J. Delasoie, A. Pavic, N. Voutier, S. Vojnovic, A. Crochet, J. Nikodinovic-Runic, F. Zobi, Identification of novel potent and non-toxic anticancer, anti-angiogenic and antimetastatic rhenium complexes against colorectal carcinoma, Eur. J. Med. Chem., 204 (2020) 112583.
[43] J.K. Stille, The Palladium-Catalyzed Cross-Coupling Reactions of Organotin Reagents with Organic Electrophiles [New Synthetic Methods (58)], Angew. Chem. Int. Ed., 25 (1986) 508-524.
[44] F. Zobi, Parametrization of the Contribution of Mono- and Bidentate Ligands on the Symmetric C O Stretching Frequency of fac-[Re(CO)(3)](+) Complexes, Inorg. Chem., 48 (2009) 10845-10855.
[45] E. Kottelat, F. Lucarini, A. Crochet, A. Ruggi, F. Zobi, Correlation of MLCTs of Group 7 fac-[M(CO)(3)](+) Complexes (M = Mn, Re) with Bipyridine, Pyridinylpyrazine, Azopyridine, and Pyridin-2-ylmethanimine Type Ligands for Rational photoCORM Design, Eur. J. Inorg. Chem., 2019 (2019) 3758-3768.
[46] G. Schanne, L. Henry, H.C. Ong, A. Somogyi, K. Medjoubi, N. Delsuc, C. Policar, F. García, H.C. Bertrand, Rhenium carbonyl complexes bearing methylated triphenylphosphonium cations as antibody-free mitochondria trackers for X-ray fluorescence imaging, Inorg. Chem. Front., 8 (2021) 3905-3915.
[47] L.D. Ramos, G. Cerchiaro, K.P. Morelli Frin, Rhenium(I) polypyridine complexes coordinated to an ethyl-isonicotinate ligand: Luminescence and in vitro anti-cancer studies, Inorg. Chim. Acta, 501 (2020) 119329.
[48] S. Clede, C. Sandt, P. Dumas, C. Policar, Monitoring the Kinetics of the Cellular Uptake of a Metal Carbonyl Conjugated with a Lipidic Moiety in Living Cells Using Synchrotron Infrared Spectromicroscopy, Appl. Spectrosc., 74 (2020) 63-71.
[49] C.C. Konkankit, B.A. Vaughn, Z. Huang, E. Boros, J.J. Wilson, Systematically altering the lipophilicity of rhenium(i) tricarbonyl anticancer agents to tune the rate at which they induce cell death, Dalton Trans., 49 (2020) 16062-16066.
[50] L.D. Ramos, L.H. de Macedo, N.R.S. Gobo, K.T. de Oliveira, G. Cerchiaro, K.P. Morelli Frin, Understanding the photophysical properties of rhenium(i) compounds coordinated to 4,7-diamine-1,10-phenanthroline: synthetic, luminescence and biological studies, Dalton Trans., 49 (2020) 16154-16165.
[51] P.T. Wilder, D.J. Weber, A. Winstead, S. Parnell, T.V. Hinton, M. Stevenson, D. Giri, S. Azemati, P. Olczak, B.V. Powell, T. Odebode, S. Tadesse, Y. Zhang, S.K. Pramanik, J.M. Wachira, S. Ghimire, P. McCarthy, A. Barfield, H.N. Banerjee, C. Chen, J.A. Golen, A.L. Rheingold, J.A. Krause, D.M. Ho, P.Y. Zavalij, R. Shaw, S.K. Mandal, Unprecedented anticancer activities of organorhenium sulfonato and

carboxylato complexes against hormone-dependent MCF-7 and hormone-independent triple-negative MDA-MB-231 breast cancer cells, Mol. Cell. Biochem., 441 (2018) 151-163.
[52] P.A. Clarke, T. Roe, K. Swabey, S.M. Hobbs, C. McAndrew, K. Tomlin, I. Westwood, R. Burke, R. van Montfort, P. Workman, Dissecting mechanisms of resistance to targeted drug combination therapy in human colorectal cancer, Oncogene, 38 (2019) 5076-5090.
[53] H. Shen, R.E. Perez, B. Davaadelger, C.G. Maki, Two 4N cell-cycle arrests contribute to cisplatin-resistance, Plos One, 8 (2013) e59848.
[54] A.A. Untereiner, A. Pavlidou, N. Druzhyna, A. Papapetropoulos, M.R. Hellmich, C. Szabo, Drug resistance induces the upregulation of H2S-producing enzymes in HCT116 colon cancer cells, Biochem. Pharmacol., 149 (2018) 174-185.
[55] P.M. De Angelis, K.L. Kravik, S.H. Tunheim, T. Haug, W.H. Reichelt, Comparison of gene expression in HCT116 treatment derivatives generated by two different 5-fluorouracil exposure protocols, Mol. Cancer, 3 (2004) 11.
[56] R. Fior, V. Póvoa, R.V. Mendes, T. Carvalho, A. Gomes, N. Figueiredo, M.G. Ferreira, Single-cell functional and chemosensitive profiling of combinatorial colorectal therapy in zebrafish xenografts, Proc. Natl. Acad. Sci. USA, 114 (2017) E8234-E8243.
[57] K. Kai, O. Nagano, E. Sugihara, Y. Arima, O. Sampetrean, T. Ishimoto, M. Nakanishi, N.T. Ueno, H. Iwase, H. Saya, Maintenance of HCT116 colon cancer cell line conforms to a stochastic model but not a cancer stem cell model, Cancer Sci., 100 (2009) 2275-2282.
[58] F. Zobi, O. Blacque, R.K.O. Sigel, R. Alberto, Binding interaction of [Re(H2O)(3)(CO)(3)](+) with the DNA fragment d(CpGpG), Inorg. Chem., 46 (2007) 10458-10460.
[59] K.M. Adams, L.G. Marzilli, fac-[Re(CO)3(H2O)3]+ Nucleoside Monophosphate Adducts Investigated in Aqueous Solution by Multinuclear NMR Spectroscopy, Inorg. Chem., 46 (2007) 4926-4936.
[60] A.V. Shtemenko, H.T. Chifotides, D.E. Yegorova, N.I. Shtemenko, K.R. Dunbar, Synthesis and X-ray crystal structure of the dirhenium complex Re2(i-C3H7COO)4Cl2 and its interactions with the DNA purine nucleobases, J. Inorg. Biochem., 153 (2015) 114-120.
[61] M. Tavares Barroso, B. Costa, C. Rebelo de Almeida, M. Castillo Martin, N. Couto, T. Carvalho, R. Fior, Establishment of Pancreatobiliary Cancer Zebrafish Avatars for Chemotherapy Screening, Cells, 10 (2021) 2077.
[62] R. White, K. Rose, L. Zon, Zebrafish cancer: the state of the art and the path forward, Nat. Rev. Cancer, 13 (2013) 624-636.
[63] F. Zobi, B. Spingler, R. Alberto, Structure, reactivity and solution behaviour of [Re(ser)(7-MeG)(CO)(3)] and [Re(ser)(3-pic)(CO)(3)]: "nucleoside-mimicking" complexes based on the fac-[Re(CO)(3)](+) moiety, Dalton Trans., (2005) 2859-2865.
[64] G.M. Sheldrick, Crystal structure refinement with SHELXL, Acta Cryst. C, 71 (2015) 3-8.
[65] G.M. Sheldrick, SHELXT - Integrated space-group and crystal-structure determination, Acta Cryst. A, 71 (2015) 3-8.
[66] C. Gütz, A. Lützen, Synthesis of 2,2’-Bipyridines via Suzuki-Miyaura Cross-Coupling, Synthesis, 2010 (2010) 85-90.
[67] T. Norrby, A. Borje, L. Zhang, B. Akermark, Regioselective functionalization of 2,2 '-bipyridine and transformations into unsymmetric ligands for coordination chemistry, Acta Chem. Scand., 52 (1998) 77-85.
[68] N.C. Fletcher, M. Nieuwenhuyzen, S. Rainey, The isolation and purification of tris-2,2’-bipyridine complexes of ruthenium(ii) containing unsymmetrical ligands, J. Chem. Soc., Dalton Trans., (2001) 2641-2648.
[69] L.-Y. Liao, X.-R. Kong, X.-F. Duan, Reductive Couplings of 2-Halopyridines without External Ligand: Phosphine-Free Nickel-Catalyzed Synthesis of Symmetrical and Unsymmetrical 2,2’-Bipyridines, J. Org. Chem., 79 (2014) 777-782.
[70] B. Imperiali, T.J. Prins, S.L. Fisher, Chemoenzymic synthesis of 2-amino-3-(2,2'-bipyridinyl)propanoic acids, J. Org. Chem., 58 (1993) 1613-1616.

[71] J. Uenishi, T. Tanaka, K. Nishiwaki, S. Wakabayashi, S. Oae, H. Tsukube, Synthesis of ι-(bromomethyl)bipyridines and related ι-(bromomethyl)pyridinoheteroaromatics: useful functional tools for ligands in host molecules, J. Org. Chem., 58 (1993) 4382-4388.
[72] S.A. Savage, A.P. Smith, C.L. Fraser, Efficient synthesis of 4-, 5-, and 6-methyl-2,2 '-bipyridine by a Negishi cross-coupling strategy followed by high-yield conversion to bromo- and chloromethyl-2,2 '-bipyridines, J. Org. Chem., 63 (1998) 10048-10051.
[73] G.R. Newkome, W.E. Puckett, G.E. Kiefer, V.D. Gupta, Y. Xia, M. Coreil, M.A. Hackney, Chemistry of heterocyclic compounds. Part 80. .alpha.-Methyl functionalization of electron-poor heterocycles. Chloromethyl derivatives of 2,2'-bipyridines, J. Org. Chem., 47 (1982) 4116-4120.
[74] M.B. Hansen, S.E. Nielsen, K. Berg, Re-examination and further development of a precise and rapid dye method for measuring cell growth/cell kill, J. Immunol. Methods, 119 (1989) 203-210.
[75] OECD, Test No. 236: Fish Embryo Acute Toxicity (FET) Test, OECD Guidelines for the Testing of Chemicals, Section 2, , OECD, (2013).
[76] C. Zhao, X. Wang, Y. Zhao, Z. Li, S. Lin, Y. Wei, H. Yang, A novel xenograft model in zebrafish for high-resolution investigating dynamics of neovascularization in tumors, Plos One, 6 (2011) e21768-e21768.